Available online at www.sciencedirect.com

ScienceDirect

Mendeleev Commun., 2023, **33**, 531–533

Mendeleev Communications

Ceramics based on double magnesium–sodium phosphates for bone regeneration

Ilya I. Preobrazhenskiy*[a] and Valery I. Putlyaev[a,b]

[a] *Department of Materials Science, M. V. Lomonosov Moscow State University, 119991 Moscow, Russian Federation. E-mail: preo.ilya@yandex.ru*

[b] *Department of Chemistry, M. V. Lomonosov Moscow State University, 119991 Moscow, Russian Federation*

DOI: 10.1016/j.mencom.2023.06.029

The fabrication of ceramics based on double phosphates $MgNaPO_4$ and $Mg_4Na(PO_4)_3$ is considered. Volume changes in phase transformations of $MgNaPO_4$ and $Mg_4Na(PO_4)_3$ upon thermal treatment in a range of 800–1100 °C and their effect on the microstructure of ceramics are studied.

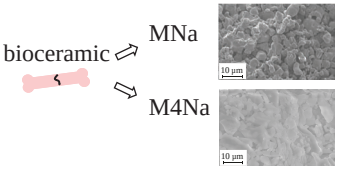

Keywords: magnesium–sodium phosphates, bioceramics, bone implants, microstructure, regenerative medicine, biomaterials.

Restoration of large bone areas while healing injuries or bone defects still remains a challenge for regenerative medicine.[1,2] Polymers[3–7] and bioceramics[8,9] are used for the regeneration of damaged bone tissues, but attention is focused on materials containing calcium phosphates because they are similar in composition to natural bone and biocompatible.[10–13] However, bioceramics based on calcium phosphates do not meet basic requirements for the materials aimed at bone healing. Ceramics and composites based on hydroxyapatite $Ca_{10}(PO_4)_6(OH)_2$ are characterized by poor solubility and a low resorption rate of ceramics during *in vivo* implantation.[14–16] From this viewpoint, magnesium phosphates can be a useful alternative to calcium phosphates due to the ability of magnesium to replace calcium in the bone mineral and bioceramics.[17] Enhanced *in vitro* and *in vivo* biodegradation of the materials based on magnesium phosphates was reported.[18,19] Thus, Ostrowski *et al.*[18] noted that amorphous magnesium phosphate pellets released up to 9 mM magnesium ions after immersion in cell culture media for 125 h, whereas the concentration of magnesium ions in a control experiment with β-tricalcium phosphate $Ca_3(PO_4)_2$ remained unchanged. The phases containing Mg^{2+} ions are promising due to their biological properties and the possibility of the formation of natural bone tissue. Magnesium is found in bone tissue, and it can replace calcium in body minerals due to their chemical similarity. Magnesium phosphates, such as newberite ($MgHPO_4{\cdot}3H_2O$) and struvite ($NH_4MgPO_4{\cdot}6H_2O$), can be used as precursors for bone implants.[20,21] The addition of 0.01 M Mg^{2+} to a cell culture medium enhanced the mineralization of an extracellular matrix.[22] Due to a greater enthalpy contribution to the hydration of cations in the course of dissolution, magnesium phosphates are characterized by a higher rate of resorption in the body environment, and they are promising biomaterials for the treatment of bone tissue defects. However, fabrication of bioceramics based on magnesium phosphates received little attention.[23,24] To tune the resorption of bioceramics, sodium cations[25,26] can be introduced into the crystal lattice of phosphates. Thus, the aim of this work was to study a relationship between phase transformations in the test double magnesium–sodium phosphates and the microstructure of corresponding ceramics.

The double magnesium–sodium phosphates were prepared using $Mg_2P_2O_7$, $Mg_3(PO_4)_2$, MgO, and Na_2CO_3 as starting materials (see Online Supplementary Materials).

The double phosphate $MgNaPO_4$ (MNa) was obtained under reported conditions[27] according to reaction (1). A mixture of magnesium pyrophosphate $Mg_2P_2O_7$ and sodium carbonate was ball-milled and then calcined in two stages at 900 and 600 °C for 10 h:

$$Mg_2P_2O_7 + Na_2CO_3 \rightarrow 2MgNaPO_4 + CO_2\uparrow. \quad (1)$$

The double orthophosphate $Mg_4Na(PO_4)_3$ (M4Na) was synthesized by solid-phase reaction (2) from the phosphate $MgNaPO_4$ and magnesium orthophosphate $Mg_3(PO_4)_2$ heated at 1100 °C for 10 h:

$$Mg_3(PO_4)_2 + MgNaPO_4 \rightarrow Mg_4Na(PO_4)_3\,. \quad (2)$$

The powder samples for dilatometric analysis were shaped by uniaxial pressing with a Carver C hydraulic manual press (see Online Supplementary Materials). Here, we report the preparation and properties of ceramics based on the double magnesium–sodium phosphates. Sintering temperatures were 800, 900, and 1000 °C. Sintering temperatures higher than 900 °C for the $MgNaPO_4$ phase caused cracks due to polymorphic transformations.[27] The crystal lattice volumes determined from powder XRD data were 916.37(4) and 950.04(2) Å^3 for MNa and M4Na powders, respectively. The powder XRD analysis of ceramic samples after calcination (Online Supplementary Materials, Figures S1 and S2) showed that a sample based on $MgNaPO_4$ sintered at 800 °C did not contain impurities of other polymorphic modifications, while the sintering temperature of 900 °C led to the appearance of impurity polymorphic modifications. It can be assumed that the high-temperature modification was a $MgNaPO_4$ phase (ICDD card 32-1121) because the intensity of its reflexes increased with temperature. At 1000 °C, $MgNaPO_4$ decomposed with the formation of $Mg_4Na(PO_4)_3$ and Na_3PO_4. Ceramic samples based on

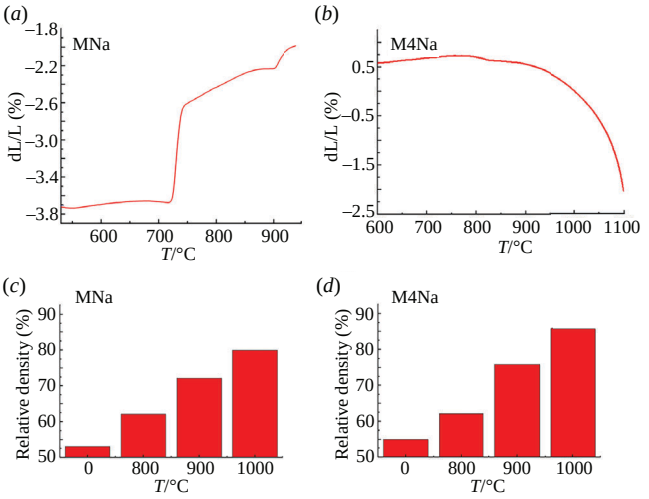

Figure 1 Linear shrinkage curves for (*a*) $MgNaPO_4$ and (*b*) $Mg_4Na(PO_4)_3$ and the bulk densities of ceramic samples after sintering at different temperatures for (*c*) $MgNaPO_4$ and (*d*) $Mg_4Na(PO_4)_3$.

$Mg_4Na(PO_4)_3$ contained reflexes related to a $Mg_4Na(PO_4)_3$ phase (ICDD card 34-671). No new phases were formed as the temperature was increased, but a decrease in the intensity of some reflexes was observed. The FT-IR spectra of powders (Online Supplementary Materials, Figure S3) showed regions of the most intense oscillations corresponding to the PO_4^{3-} (at 900–1200 cm^{-1}) and Mg–O (at 565 cm^{-1}) groups.[28]

Dilatometry was used to reveal volume changes during the heating of ceramic samples [Figures 1(*a*),(*b*)]. The thermal behavior of ceramics is important for optimizing sintering temperatures because volume changes can cause cracking and reduce the strength characteristics. Shrinkage curves for the phosphate $MgNaPO_4$ correlated with thermal analysis data.[27] Thus, volume changes at 722 and 902 °C in the DTA curve were undoubtedly associated with phase transitions. The volume change $\Delta V/V$ at 722 °C was about 3.1%, and this expansion upon heating may lead to heavy cracking of the ceramics. However, the volume change at 902 °C was significantly at a level of 0.7%, and the resulting stress was not so crucial in sense of cracking. The $Mg_4Na(PO_4)_3$ phase decomposed at >1040 °C, and the dilatometry temperature was limited to 1100 °C. We have discovered a dangerous change of about 2% in the volume at 1025 °C due to a phase transition, which was also confirmed by DTA. Thus, we observed phase transitions of $MgNaPO_4$ at 722 and 902 °C with volume changes of 3.1 and 0.7%, respectively, and $Mg_4Na(PO_4)_3$ at 1025 °C with a volume change of about 2% and the decomposition of $Mg_4Na(PO_4)_3$ at >1040 °C.

Evidently, the values of bulk and linear shrinkage increased with temperature [Figures 1(*c*),(*d*)]. The highest bulk densities were observed upon heating at 1000 °C [82 and 85% for $MgNaPO_4$ and $Mg_4Na(PO_4)_3$, respectively]. Samples of $Mg_4Na(PO_4)_3$ sintered at 800 °C were highly brittle because this temperature was insufficient for obtaining dense and tough ceramics. Heating at 900 °C led to shrinkages of 11 and 10% for the ceramics based on $MgNaPO_4$ and $Mg_4Na(PO_4)_3$, respectively.

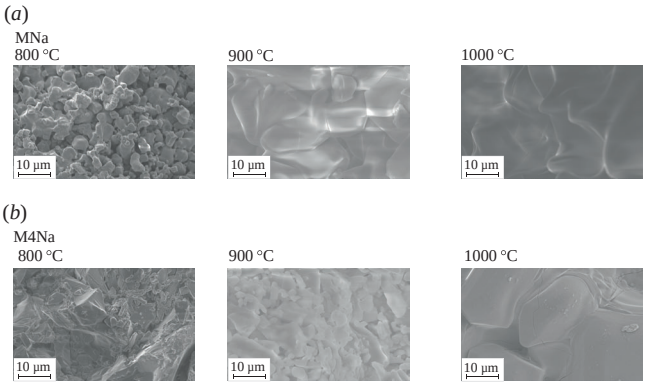

Figure 2 Microstructure of the ceramics based on (*a*) $MgNaPO_4$ and (*b*) $Mg_4Na(PO_4)_3$ after sintering at different temperatures.

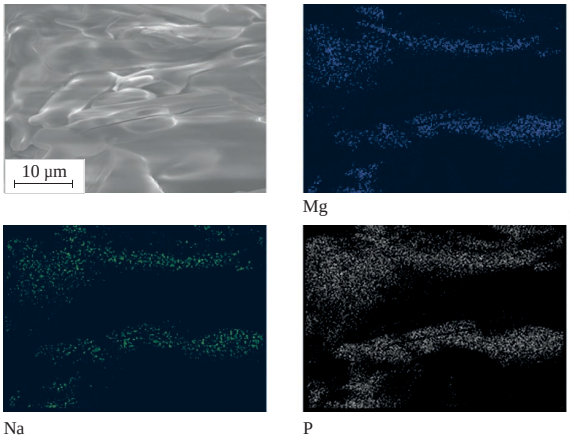

Figure 3 EDX element maps (Mg, Na, and P) of the ceramic material based on $MgNaPO_4$ sintered at 1000 °C.

Figure 2 shows the microstructure of the ceramic samples. The $MgNaPO_4$ ceramics sintered at 800 °C had an average grain size of 5 μm. Upon sintering at 900 °C, cracks in the ceramics became evident due to a phase transition in $MgNaPO_4$. Melt traces were visible at 1000 °C because the rate of recrystallization was greater than the rate of densification. An optimal calcination temperature for $MgNaPO_4$ was 800 °C, which is lower than the phase transition temperature. Upon heating $Mg_4Na(PO_4)_3$ at 1000 °C, a dense microstructure consisting of tightly bound hexagonal-like grains was formed; however, the formation of cracks was observed. A sintering temperature of 900 °C can be optimal because it does not exceed the temperature of phase transformations and makes it possible to obtain dense ceramics.

The distribution of elements across the samples was studied by elemental mapping based on energy dispersive X-ray spectroscopy (EDX analysis).[29] Figure 3 shows uniform distributions of magnesium and sodium across the samples of sintered ceramics.

Thus, we studied the sintering of ceramic materials based on double magnesium–sodium phosphates. The sintering of $Mg_4Na(PO_4)_3$ ceramics at 800 °C was accompanied by poor densification, which made it impossible to reach reasonable strength of the ceramics. At the same time, a sintering temperature of 1000 °C was too high and led to the appearance of cracks inside the ceramics because it is close to the temperature of a polymorphic transformation in $Mg_4Na(PO_4)_3$. The ceramic materials based on $MgNaPO_4$ should be sintered at 800 °C; this temperature allows one to avoid cracking and changing the phase composition of ceramics.

This work was supported by the Russian Science Foundation (grant no. 22-19-00219). A part of the used equipment was purchased through the Program of Lomonosov Moscow State University Development.

Online Supplementary Materials

Supplementary data associated with this article can be found in the online version at doi: 10.1016/j.mencom.2023.06.029.

References

1 A. Przekora, *Int. J. Mol. Sci.*, 2019, **20**, 435.
2 F. Donnaloja, E. Jacchetti, M. Soncini and M. T. Raimondi, *Polymers*, 2020, **12**, 905.

3 E. V. Razuvaeva, K. T. Kalinin, N. G. Sedush, A. A. Nazarov, D. S. Volkov and S. N. Chvalun, *Mendeleev Commun.*, 2021, **31**, 512.
4 I. I. Preobrazhenskiy and V. I. Putlyaev, *Mendeleev Commun.*, 2023, **33**, 83.
5 S. Ghosh, S. Mukherjee, D. Patra and J. Haldar, *Biomacromolecules*, 2022, **23**, 592.
6 I. I. Preobrazhenskii and V. I. Putlyaev, *Russ. J. Appl. Chem.*, 2022, **95**, 775 (*Zh. Prikl. Khim*., 2022, **95**, 685).
7 I. I. Preobrazhensky, A. A. Tikhonov, E. S. Klimashina, P. V. Evdokimov and V. I. Putlyaev, *Russ. Chem. Bull.*, 2020, **69**, 1601.
8 A. Ezerskyte-Miseviciene and A. Kareiva, *Mendeleev Commun.*, 2019, **29**, 273.
9 Q. Liu, T. Li, S. W. Gan, S. Y. Chang, C. C. Yen and W. Zhai, *Addit. Manuf.*, 2023, **61**, 103332.
10 M. A. Goldberg, V. V. Smirnov, O. S. Antonova, D. R. Khairutdinova, S. V. Smirnov, A. I. Krylov, N. S. Sergeeva, I. K. Sviridova, V. A. Kirsanova, S. A. Akhmedova, S. N. Zhevnenko and S. M. Barinov, *Mendeleev Commun.*, 2018, **28**, 329.
11 I. I. Preobrazhenskiy, A. A. Tikhonov, P. V. Evdokimov, A. V. Shibaev and V. I. Putlyaev, *Open Ceram.*, 2021, **6**, 100115.
12 I. V. Fadeeva, M. A. Goldberg, I. I. Preobrazhensky, G. V. Mamin, G. A. Davidova, N. V. Agafonova, M. Fosca, F. Russo, S. M. Barinov, S. Cavalu and J. V. Rau, *J. Mater. Sci.: Mater. Med*., 2021, **32**, 99.
13 D. R. Khayrutdinova, O. S. Antonova, M. A. Golgberg, S. V. Smirnov, P. A. Krokhicheva, S. M. Barinov and V. S. Komlev, *Dokl. Chem.*, 2020, **493**, 117 (*Dokl. Ross. Akad. Nauk. Khim., Nauki Mater.*, 2020, **492**–**493**, 50).
14 M. C. Tronco, J. B. Cassel and L. A. Dos Santos, *Acta Biomater.*, 2022, **151**, 70.
15 I. V. Fadeeva, A. S. Fomin, S. M. Barinov, G. A. Davydova, I. I. Selezneva, I. I. Preobrazhenskii, M. K. Rusakov, A. A. Fomina and V. A. Volchenkova, *Inorg. Mater.*, 2020, **56**, 700 (*Neorg. Mater*., 2020, **56**, 738).
16 Y. Wang, X. Yuan, J. Ye and F. He, *Ceram. Int.*, 2022, **48**, 28557.
17 J. Zhang, L. Tang, H. Qi, Q. Zhao, Y. Liu and Y. Zhang, *Adv. Healthcare Mater.*, 2019, **8**, 1901030.
18 N. Ostrowski, B. Lee, D. Hong, P. N. Enick, A. Roy and P. N. Kumta, *ACS Biomater. Sci. Eng.*, 2015, **1**, 52.
19 U. Klammert, A. Ignatius, U. Wolfram, T. Reuther and U. Gbureck, *Acta Biomater.*, 2011, **7**, 3469.
20 F. Kaiser, L. Schröter, S. Stein, B. Krüger, J. Weichhold, P. Stahlhut, A. Ignatius and U. Gbureck, *Acta Biomater.*, 2022, **145**, 358.
21 P. Sikder, S. B. Bhaduri, J. L. Ong and T. Guda, *J. Biomed. Mater. Res., Part B*, 2020, **108**, 976.
22 S. Yoshizawa, A. Brown, A. Barchowsky and C. Sfeir, *Acta Biomater.*, 2014, **10**, 2834.
23 K. Sarkar, M. Rahaman, S. Agarwal, S. Bodhak, S. Halder, S. K. Nandi and M. Roy, *Mater. Lett.*, 2020, **259**, 126892.
24 T. M. Bedair, Y. Heo, J. Ryu, H. M. Bedair, W. Park and D. K. Han, *Biomater. Sci.*, 2021, **9**, 1903.
25 A. A. Gutsalova, D. A. Fedorishin, D. N. Lytkina and I. A. Kurzina, *Mendeleev Commun.*, 2021, **31**, 382.
26 A. Namdar and E. Salahinejad, *Coord. Chem. Rev.*, 2023, **478**, 215001.
27 I. I. Preobrazhenskiy and V. I. Putlyaev, *Inorg. Mater.*, 2022, **58**, 349 (*Neorg. Mater*., 2022, **58**, 367).
28 J. Barralet, S. Best and W. Bonfield, *J. Biomed. Mater. Res.*, 1998, **41**, 79.
29 H. Rasouli and H. Esmaeili, *3 Biotech*, 2019, **9**, 429.

Received: 13th March 2023; Com. 23/7116